Full paper

# High-performance triboelectric nanogenerators for self-powered, in-situ and real-time water quality mapping

Yu Bai[a,b,1], Liang Xu[a,b,1], Chuan He[b,c,1], Laipan Zhu[a,b], Xiaodan Yang[a,b], Tao Jiang[a,b], Jinhui Nie[a,b], Wei Zhong[a,b], Zhong Lin Wang[a,b,d,*]

[a] CAS Center for Excellence in Nanoscience, Beijing Key Laboratory of Micro-Nano Energy and Sensor, Beijing Institute of Nanoenergy and Nanosystems, Chinese Academy of Sciences, Beijing, 100083, China
[b] School of Nanoscience and Technology, University of Chinese Academy of Sciences, Beijing, 100049, China
[c] School of Materials Science and Engineering, Beijing Institute of Technology, Beijing, 100081, China
[d] School of Material Science and Engineering, Georgia Institute of Technology, Atlanta, GA, 30332, USA

ABSTRACT

Water pollution is one of the most severe environmental issues nowadays. For sustainably and autonomously monitoring water quality, in-situ self-powered sensing systems which can harvest local wave energy are highly desired. Here, a high-performance tandem disk triboelectric nanogenerator (TD-TENG) for self-powered water quality monitoring is demonstrated. By surface modification and optimized design, a radial grating structure which can be effectively agitated by slow water waves is realized, boosting the peak and average power of wave-energy-harvesting TENG devices to 45.0 mW and 7.5 mW respectively, which are roughly 35 and 24 folds of the typical ball-shell structured device. The average power density reaches $7.3 \, \mathrm{W \, m^{-3}}$, setting up a new record. The short-circuit current is greatly enhanced to 11 mA through a facile power management circuit. The high output enables a self-powered total dissolved solids testing system, which can be scaled up into networks for in-situ, real-time mapping water quality in a large area. The TD-TENG as a high-power wave energy harvesting device also opens up an avenue to solve the bottleneck of power supply for versatile sensing platforms that need to work autonomously in water, providing a fundamental technology for smart environmental and ocean science.

## 1. Introduction

Water covers more than 70% of the earth's surface. It is the most essential element for living things, and also influences profoundly weather systems, geographical structures and so on. Despite its significance, water pollution has been one of the most severe environmental issues nowadays. The major pollutants include fertilizers, pesticides, sewage, oils, heavy metals, trace elements, plastics, eutrophication and so on [1,2]. A series of problems have arisen as a result of water pollution: death of the aquatic organisms, degradation of coastal and marine habitat, reduction of economic benefits, even some toxic substances are transported to human through food chain, causing public health risk [2,3]. In order to detect, analyze and control water pollution effectively, it is necessary to develop water quality monitoring systems that can work in-situ and real-time.

Recent advances on water quality monitoring mainly focus on the

development of sensors [4–8]. Actually, how to power these sensors is also a critical problem. Such sensors distributed in vast water environment are always not convenient to be powered through cables. A battery can only last limited time and needs to be charged, which is costly and inconvenient and unsustainable. Solar panel can solve some of the problem. However, its performance is strongly affected by weather, day and night, and cannot be used underwater. Thus harvesting energy conserved locally in water, namely the wave energy, should be a promising choice. The wave energy distributes vastly in water bodies, and it is less affected by the alternate of day and night and weather [9–11]. Through harvesting wave energy from surrounding water environment, the sensor could be effectively driven, enabling self-powered, in-situ water quality monitoring in a sustainable and autonomous way.

The triboelectric nanogenerator (TENG) is proved to be an effective device for harvesting water wave energy [9]. Invented in 2012, TENGs

with a variety of structure designs and material choices have been successfully developed to convert various mechanical energy into electrical energy [12–22]. The working mechanism of the TENG is based on triboelectrification and electrostatic induction, which can trace its fundamental from the Maxwell's displacement current [23,24]. Compared with traditional electromagnetic generators, the TENG has merits of light weight, easy fabrication, low cost, and versatile material and structure choices [14,24–26]. Considering the tremendous conservation on earth, the blue energy, which adopts TENG networks to harvest wave energy, is regarded as one of the major application fields of the TENG [24,27,28]. Previous works have reported a few prototypes which successfully realized wave energy harvesting in principle, and small electronics such as thermo meters and wireless transmitters are driven by the harvested energy [9,29–32]. To power water quality sensors that have much larger power consumption, TENGs with much higher power output, especially the average power, is needed which is a great challenge. The radial grating disk structure is regarded as a high-power structure for the TENG [33]. However, it is difficult to be applied in water wave energy harvesting due to the large friction force between disks that almost cannot be driven by the low-frequency and slow water wave motion.

In this work, an expandable tandem disk triboelectric nanogenerator (TD-TENG) based on radial grating disk structure is demonstrated for self-powered water quality monitoring. Designs of swinging mass blocks and surface modification are adopted to enable effective agitation of the device by slow water waves, converting low-frequency water wave agitations into high-frequency electrical output to enhance the average power. With optimized design, the device boosts the output with a maximum peak power of 45.0 mW and a maximum average power of 7.5 mW in wave tank tests, which are roughly 35 folds and 24 folds of the ball-shell structured device [31]. The average power density reaches 7.3 W m$^{-3}$. Moreover, the short-circuit current is enhanced to 11 mA through a facile power management circuit, which is a great advance as compared to reported current at the level of tens or hundreds microampere. Such high output is enough to drive water quality monitoring. A self-powered total dissolved solids (TDS) testing system is demonstrated, which can be scaled up into networks for in-situ, real-time mapping water quality in a large area. The TD-TENG as a high-power water wave energy harvesting device should provide a fundamental technology for future ocean research and exploiting, such as environment protection, smart ocean and wave energy farm.

## 2. Results and discussion

### 2.1. Device structure and working principle

Fig. 1a demonstrates a schematic diagram of a self-powered water quality monitoring system. The system consists of a water quality sensor (without a battery) and a TENG. The TENG extracts wave energy from the water, producing electricity which is further converted into an appropriate form by power management. Then the sensor can be powered with the harvested energy and water quality information can be collected sustainably without extra efforts on maintaining batteries. To realize such self-powered system, the TD-TENG based on a rotary radial electrode structure is designed, as shown in Fig. 1b. TENG units arranged in tandem with two hanging mass blocks (550 g for each block) on both sides are packaged by a water-proof acrylic shell. Each TENG unit is composed by the facing sides of a rotator disk and a stator disk (Fig. 1c). All the stators are fixed on the acrylic shell, and all the rotators are connected with the hanging blocks by two shafts to ensure synchronous movement. The blocks are designed in an eccentric form which can response to the agitation of water waves and drive the rotation of the rotators. The amount of triboelectric disks is expandable, and 21 disks are integrated in our device here, which form 20 units in total. Fig. 1d depicts the details of the rotator and the stator. For the rotator, two Cu layers with equally-spaced radial-arrayed sectors were

coated on both sides of a frosted acrylic substrate using magnetron sputtering and act as electropositive triboelectric materials. The periodicity of the radial grating is 7.5°. As for the stator, firstly, two Cu layers with complementary-patterned sectors were fabricated through the printed circuit board (PCB) technology on both sides of a substrate made of epoxy glass fiber, forming two electrodes on each side with the same periodicity as the rotator. Polytetrafluoroethylene (PTFE) films were adhered on the electrodes as electronegative triboelectric materials. The photographs of the stator without PTFE films at different magnifications are shown in Fig. 1e–i, ii, and iii, and Fig. 1e–iv gives the photograph of the frosted acrylic without Cu. The scanning electron microscope (SEM) images of the surface of the frosted acrylic are presented in Fig. 1e–v and vi. Here, frosted acrylic with rough surface is adopted to control the friction force by reducing the contact area, because smooth surface always experiences too large friction force which prohibits the rotator from rotation in low-frequency water waves. As compared in Figs. S1–S4, the friction force is largely reduced by 58% for the frosted acrylic with the trade-off of some charge output deduction (45%). Actually, the rotator of smooth acrylic can be easily locked by high friction force with the stator, due to mutual reinforcement of electrostatic charges (that attracts two surfaces) and friction force. In such a case, the rotator cannot be agitated by water waves and the output is even zero. Thus limiting the friction force is the key for the device which is well achieved by the frosted surface structure. The abrasion for the frosted acrylic is also greatly suppressed with better durability (Fig. S2). Details of the fabrication process of the TD-TENG can be found in the Experimental Section. Fig. 1f shows the basic working mechanism of the TENG unit, which is based on the conjugation of triboelectrification and electrostatic induction. By rotary triboelectrification, the isolated Cu layer (showing one section in Fig. 1f) on the rotator will be positively charged and the surface of the PTFE film will be negatively charged. With the relative rotation of the rotator and the stator, the movement of the positively charged Cu section would induce charge transferring between the two electrodes through an external circuit, producing current.

### 2.2. Electrical characterization under harmonic agitations

To understand fundamental output characteristics of the TD-TENG, we applied two basic forms of agitations by a linear motor. The first agitation form is shown in Fig. 2a. The rotators were fixed and the stators were driven by the motor, thus only the relative rotation between the rotators and the stators were considered. The motor conducted a reciprocating linear motion in a sinusoidal way, which was converted into a reciprocating rotation for the stators by a pinion and rack mechanism with a conversion ratio of 1.43 deg/mm. The electrical output, i.e. the open-circuit voltage ($V_{oc}$), short-circuit current ($I_{sc}$) and short-circuit transferred charges ($\Delta Q$) were evaluated systematically. For the TD-TENG, one side of the rotator and the adjacent side of the stator are coupled as one basic unit (see Fig. 1f), and the outputs of the units are parallel connected to produce the total output. In Fig. 2b and c, the $I_{sc}$ and $\Delta Q$ of the TD-TENG with different numbers of units (1, 4, 8, 12, 16, and 20) are presented respectively. The driving frequency is 0.75 Hz and the amplitude is 30 mm (The amplitude is defined as the moving extent of the linear motor here). As can be observed, with increasing number of units, the peak value of $I_{sc}$ increases from 8 μA to 120 μA, and $\Delta Q$ increases from 0.2 μC to 3.4 μC almost in a linear way. The results indicate that by simply connecting more units the electrical output of the TD-TENG can be further scaled up. The detailed profiles of the $V_{oc}$, $I_{sc}$, and $\Delta Q$ of the TD-TENG with 20 units in one motor cycle are shown in Fig. 2d, e, and f, respectively. The peak-to-peak value of the $V_{oc}$ can reach 365 V. Moreover, owing to the grating structure of the electrode and the triboelectric material, the electrical signals exhibit a frequency-multiplication effect to the external agitation, and a high-frequency electrical output is obtained by low-frequency mechanical agitations, which can greatly enhance the average power output of the
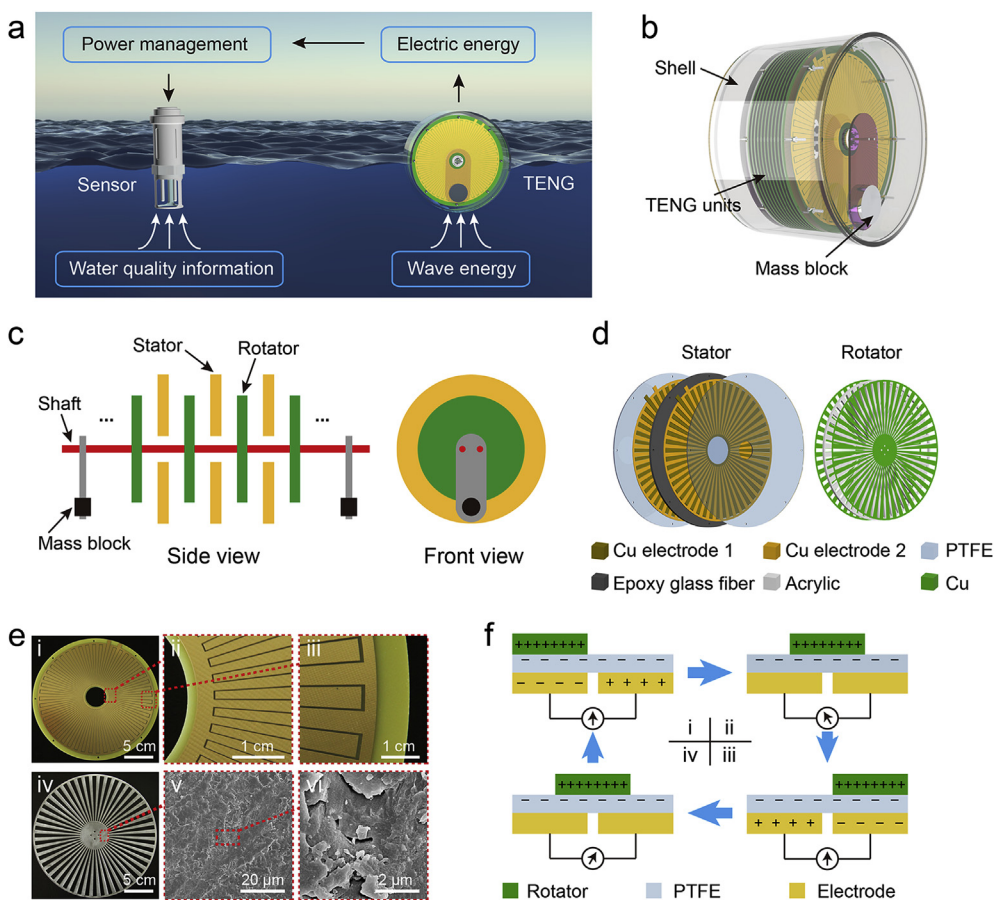
**Fig. 1.** Structure and working principle of the TD-TENG. a) Schematic diagram of the self-powered water quality monitoring system. b) Overview of the structure of the TD-TENG. c) Schematic illustration of the side view and front view of the TD-TENG. d) Material composition of the TD-TENG. e) Photographs and SEM images of the (i-iii) stator without PTFE films and (iv-vi) rotator without Cu: (i) photograph of the stator, (ii-iii) enlarged photographs of different parts of the electrodes, (iv) photograph of the rotator, (v-vi) SEM images of the frosted surface of the rotator at different scale. f) Schematics of working principle of the TENG unit.
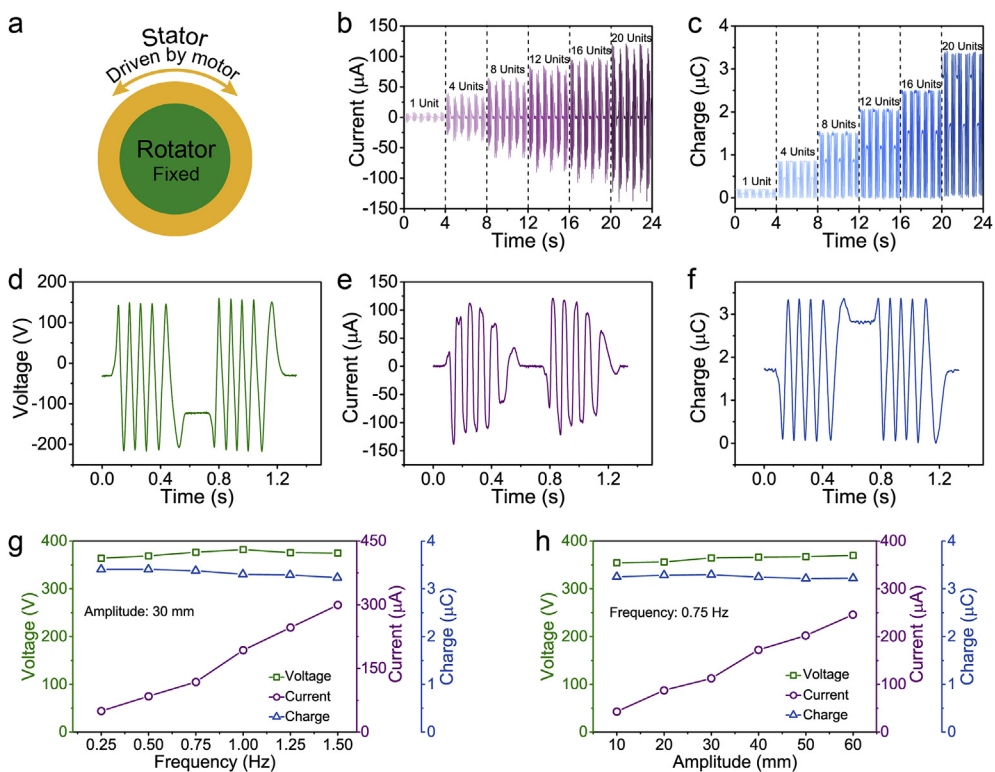


**Fig. 2.** Electrical measurements of the TD-TENG under simple relative rotation. a) Schematic illustration of the motion state of the rotator and the stator. b) Short-circuit current and c) transferred charges of the device when different amounts of TENG units are connected in parallel. d) Open-circuit voltage, e) short-circuit current, and f) transferred charges of the TD-TENG in one motor cycle. (b–f) are all measured under an amplitude of 30 mm and a frequency of 0.75 Hz. g) The output of the TD-TENG under different frequencies. h) The output of the TD-TENG under different amplitudes.
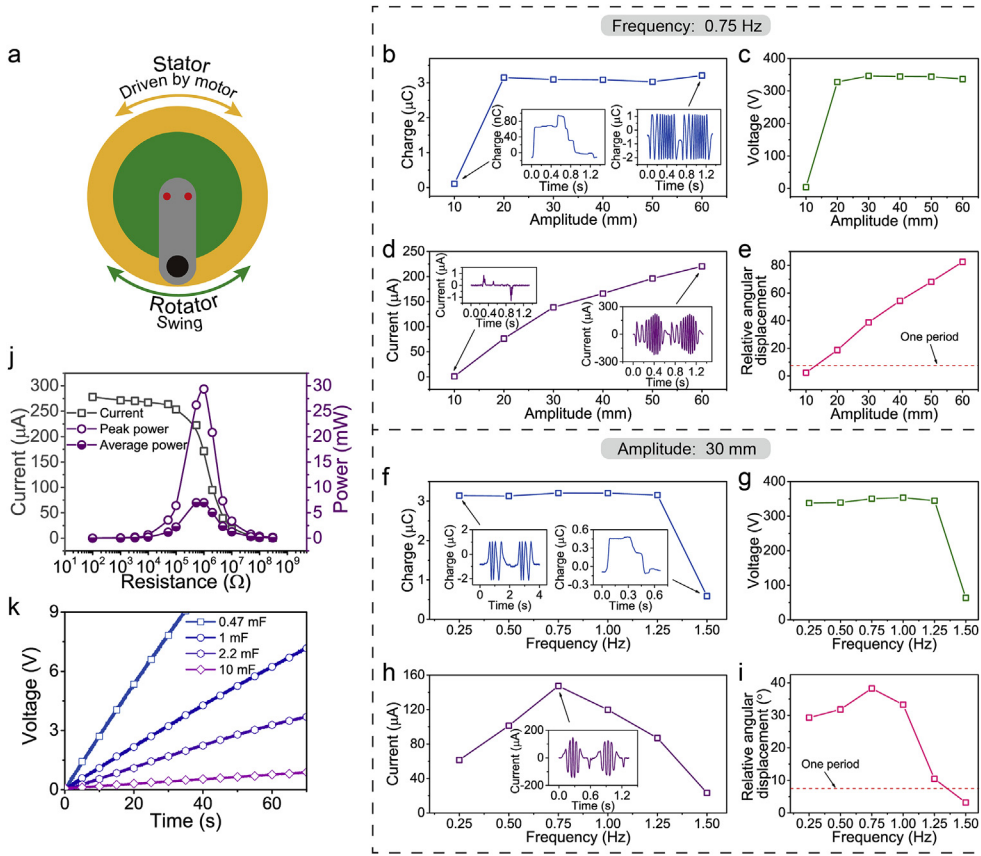
**Fig. 3.** Electrical measurements of the TD-TENG with the rotator swinging freely. a) Schematic illustration of the motion state of the rotator and the stator of the TD-TENG under different amplitudes. b-d) The electrical output and e) the relative angular displacement of the rotator and the stator of the TD-TENG under different amplitudes. f-h) The electrical output and i) the relative angular displacement of the rotator and the stator of the TD-TENG under different frequencies. The insets show details of the output curves in one motor cycle. j) The peak current, peak power and average power of the TD-TENG under various loads. k) The voltage of different capacitors charged by the TD-TENG. (j, k) are tested under a frequency of 1 Hz and an amplitude of 60 mm.

device as will be discussed later. Here, at least 8 output cycles can be observed in only one motor cycle, and this will be even higher with larger amplitude.

Fig. 2g and h shows the dependence of the output on the driving frequency and amplitude. As the frequency increases from 0.25 to 1.5 Hz (Fig. 2g), the peak-to-peak value of $V_{oc}$ and the peak value of $\Delta Q$ remain steady at around 373 V and 3.3 μC respectively, while the peak value of $I_{sc}$ increases almost linearly with the frequency, reaching up to 299 μA at the frequency of 1.50 Hz. For varying amplitude from 10 to 60 mm (Fig. 2h), the peak-to-peak value of $V_{oc}$ and the peak value of $\Delta Q$ stay around 363 V and 3.3 μC respectively, while the peak value of $I_{sc}$ increases up to 246 μA. The characteristics originate from the periodic radial grating feature of the device. The $V_{oc}$ and $\Delta Q$ are related to the relative motion of the rotator and the stator and achieve the maximum if one period of the radial grating is reached [33,34]. Here, the relative motion is larger than one such period, thus the peak values of the $V_{oc}$ and $\Delta Q$ are always the maximum value in one period. The $I_{sc}$ is related to the velocity of the relative motion according to $I = dQ/dt$, so it will alter obviously with varying frequency or amplitude.

After evaluating the electrical performance of the TD-TENG under simple relative rotation between the rotator and the stator, another agitation form was introduced to simulate the motion of the device in water waves, where the rotator and the block swing freely as the stator rolls sinusoidally under the driving of the motor, as shown in Fig. 3a. The dependences of the $\Delta Q$, $V_{oc}$ and $I_{sc}$ of the TD-TENG on the driving amplitude are presented in Fig. 3b, c and d, respectively. As the driving amplitude of the linear motor increases, the peak value of $I_{sc}$ also rises, while the peak-to-peak value of $V_{oc}$ and the peak value of $\Delta Q$ remain almost unchanged, except for the case at the amplitude of 10 mm, where the relative angular displacement is lower than one period (7.5°) of the radial grating, as illustrated in Fig. 3e. Comparison of the signal profiles presented in the insets of Fig. 3b and d can further support the above discussion.

Similarly, the dependences of the $\Delta Q$, $V_{oc}$ and $I_{sc}$ of the TD-TENG on the driving frequency are presented in Fig. 3f, g and h respectively. As the frequency rises, the peak value of $I_{sc}$ first increases and then decreases, and the maximum $I_{sc}$ of 147 μA occurs at the frequency of about 0.75 Hz, corresponding to the maximum relative angular displacement (Fig. 3i). For larger frequency, the device cannot response adequately to the fast external agitation, thus the relative angular displacement decreases. However, this will not affect its performance in harvesting wave energy which is mainly in low frequency. The peak-to-peak value of $V_{oc}$ and the peak value of $\Delta Q$ remain almost steady, except for the one at the frequency of 1.50 Hz, where the relative angular displacement is lower than one period of the radical grating (Fig. 3i).

To characterize the power of the TD-TENG, the electrical output of the device was measured using resistors as external loads at the driving frequency of 1 Hz and the amplitude of 60 mm. As shown in Fig. 3j, when the load resistance increases, the peak value of the $I_{sc}$ decreases as a result of Ohmic loss, and a maximum peak power of 29.4 mW and maximum average power of 7.0 mW are achieved at a matched load resistance of about 1 MΩ. The average power is calculated according to the following equation:

$$P_{ave} = \frac{\int_0^T I^2 R dt}{T} \tag{1}$$

where $I$ is the output current, $T$ is the period and $R$ is the load. The matched resistance is relatively low due to the tandem structure of the TD-TENG which has relative low internal impedance with many units parallel connected [23]. The charging performance of the TD-TENG for different capacitors was also investigated. The voltage curves for 0.47, 1, 2.2 and 10 mF capacitors charged by the TD-TENG at the driving frequency of 1 Hz and the amplitude of 60 mm are shown in Fig. 3k. The 0.47 mF capacitor could be charged to 9 V in 35 s, while the 1, 2.2 and 10 mF capacitors were charged to 7.1, 3.7, and 0.89 V respectively, in 70 s.
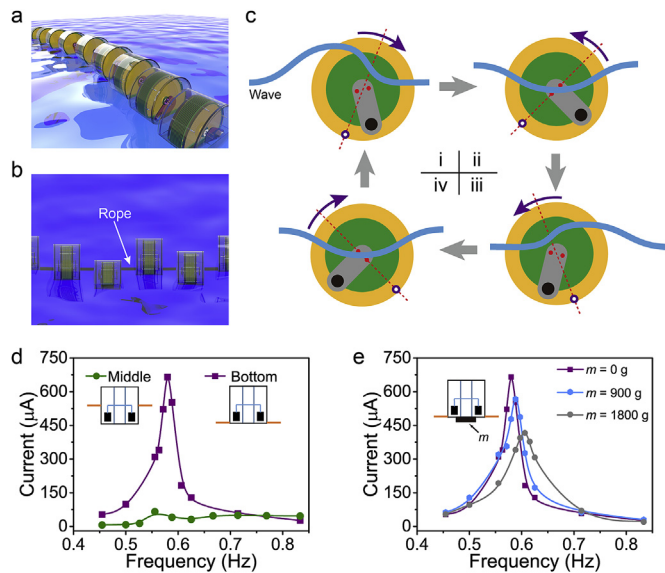
**Fig. 4.** Optimization of the TD-TENG network in water. a, b) Schematic illustrations of connected TD-TENGs in water. c) Working principle of the TD-TENG in water. d) Short-circuit current of the TD-TENG with different positions of connecting point under various frequencies of the waves. e) Short-circuit current of the TD-TENG with different additional mass blocks under various frequencies of the waves.

### 2.3. Device optimization and electrical measurements in water

The above experimental results demonstrate the capability of the TD-TENG as an effective energy harvester for low-frequency agitations. When applied in water wave energy harvesting, the device is designed to be connected in strings and then forms a network to harvest large-scale wave energy and to be anchored, as schematically demonstrated in Fig. 4a and b. The basic agitation process of a single device in a network is illustrated in Fig. 4c. The device is constrained by the rope from the bottom and can rotate around the connecting point, similar to the second situation driven by the motor. When agitated by water waves, the block together with the rotator will swing freely as the stator and the shell move around the bottom connecting point. Details of one cycle can be roughly divided into four stages: firstly, the water wave at

the left side will push the TD-TENG to swing to the right (Fig. 4c–i), and the device will move back after reaching the rightmost point due to the buoyancy (Fig. 4c–ii); if the swing frequency is consistent with the wave frequency, the neighboring wave at the right side will assist in the backward swing motion (Fig. 4c–iii); then the device swings to its leftmost point inertially and floats back into the original state (Fig. 4c–iv). With repeating swing of the device, the eccentric mass block will swing like a pendulum to drive the rotator, harvesting the wave energy and producing electricity.

In nature, the major frequency of the water wave is typically below 2 Hz [9]. To improve the energy harvesting efficiency, it is important to match the frequency characteristics of the TD-TENG with the wave. We investigated the dependence of the frequency response under different configurations concerning the position of the connecting point and additional mass block, as shown in Fig. 4d and e. The experiments were conducted in a wave tank where nine wave makers were adopted to generate waves. First, configurations with different positions of the connecting point were tested (Fig. 4d). Compared to the connecting at the bottom, the middle connection produces much smaller output which can be attributed to the symmetric configuration of the shell relative to the rotation pivot as is difficult to be pushed to swing by the waves. The output with bottom connection shows obvious frequency-dependence and reaches the maximum peak $I_{sc}$ of 650 μA at about 0.58 Hz. The influence of the additional block at the bottom of the TD-TENG was also studied. As can be observed in Fig. 4e, with the mass of the block increasing, the resonant frequency of the device and the bandwidth also rises, while the peak of $I_{sc}$ decreases. This indicates that the additional mass can be a way to tune the frequency characteristics of the device and the feature of low-frequency response can match the frequency of water waves very well. To obtain a better power output performance, we adopted the configuration of bottom connection with no additional block attached in later experiments.

The electrical output of the TD-TENG in water waves was characterized at the driving frequency of 0.58 Hz. Fig. 5a, b and c show the $V_{oc}$, $I_{sc}$ and $\Delta Q$ of the TD-TENG in two periods, respectively. The peak-to-peak value of the $V_{oc}$ and the peak of $\Delta Q$ remain around 335 V and 3.3 μC, which are close to previous results. The $I_{sc}$ of the TD-TENG is closely related to the velocity of the relative rotation between the rotator and the stator, thus the fluctuation of output signal in Fig. 5b should originate from the varying motion condition of the TD-TENG as it swings back and forth in water waves. The charging performance of
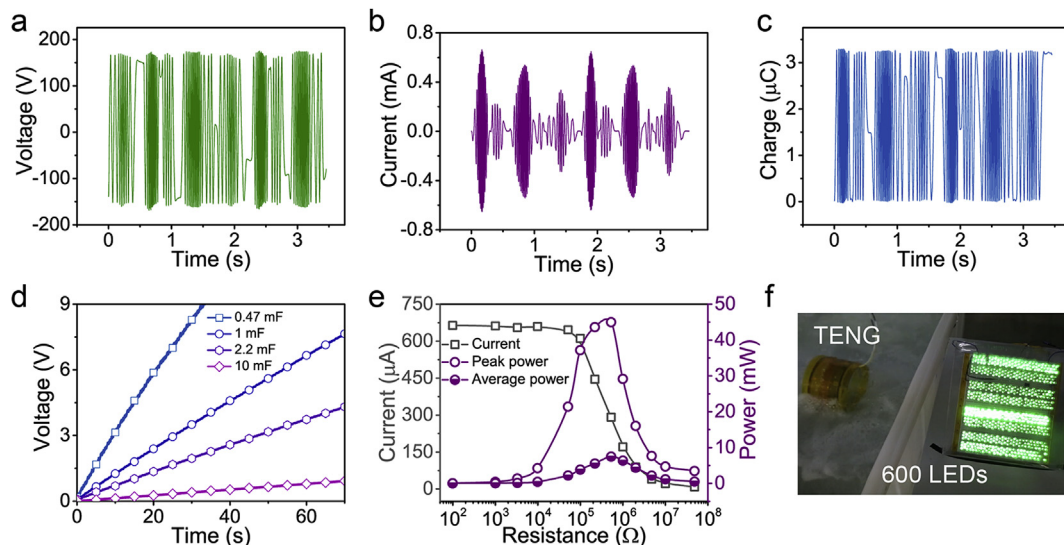


**Fig. 5.** Electrical measurements of the TD-TENG in water. a) Open-circuit voltage, b) short-circuit current and c) transferred charges of the TD-TENG in water. d) The voltage of different capacitors charged by the TD-TENG in water. e) The peak current, peak power and average power of the TD-TENG under various loads in water. f) 600 LEDs lighted directly by the TD-TENG. The wave frequency is 0.58 Hz.

the TD-TENG to different capacitors was also investigated. Fig. 5d compares the voltage curves of 0.47, 1, 2.2 and 10 mF capacitors charged by the TD-TENG. The 0.47 mF capacitor was charged to 9 V in 33 s, and the 1, 2.2 and 10 mF capacitors were charged to 7.6, 4.3 and 0.9 V, respectively, in 70 s. The electrical output of the TD-TENG with different external loads at the wave frequency of 0.58 Hz is shown in Fig. 5e. The maximum peak power and maximum average power reaches 45.0 mW and 7.5 mW, roughly 35 folds and 24 folds of the peak power and average power of the ball-shell structured device, respectively [31]. The average power density is 7.3 W m$^{-3}$ when only the volume of TENG units is considered, and 1.3 W m$^{-3}$ when the volume of the whole device is calculated. With more TENG units integrated, the inner volume of the device can be utilized more efficiently which can further improve the power density for the whole device. The achieved average power output here is much higher than previously reported results [9,31,35], which can be partly attributed to the frequency-multiplication effect of the TD-TENG that converts low-frequency wave agitations into high-frequency electrical signals with high average output. To intuitively demonstrate the capability of the TD-TENG as an energy harvester and power source, commercial light-emitting diodes (LEDs) were directly connected to the TD-TENG as the load. As shown in Fig. 5f and Video S1, 600 LEDs can be lighted up simultaneously by a single TD-TENG.

Supplementary video related to this article can be found at https://doi.org/10.1016/j.nanoen.2019.104117.

## 2.4. Power management and water quality mapping

The high performance of the TD-TENG is ready for the self-powered water quality monitoring system. To further improve the efficiency and match the requirements of electronics, power management circuit is adopted between the device and the load, lowering the output voltage and enhancing the current, as demonstrated in Fig. 6a. Due to the output of the TD-TENG is in the form of alternating current with relative high frequency, it is feasible to adopt a facile method using only a transformer and a rectifier without any complex circuit [36,37]. The transformer boosts the output current and concomitantly decreases the voltage of the TD-TENG, as shown in Fig. 6b and c. The transformed output can then be rectified by the rectifier into direct current, which can be stored in capacitors or batteries and powers electronics for monitoring the water quality. Fig. 6d compares the $V_{oc}$ and $I_{sc}$ of the TD-TENG with and without a transformer at the wave frequency of 0.58 Hz in wave tank experiments. After the transformation, the maximum peak value of the $I_{sc}$ increases from 650 μA to 11 mA, while the maximum peak-to-peak value of the $V_{oc}$ decreases from 335 V to 27 V. The charging performance of the device to capacitors with and without power management is also compared, as shown in Fig. 6e. With power management, the initial charging rate is boosted to 3.1 folds for the capacitor of 1 mF and 6.3 folds for 10 mF, which can greatly improve the efficiency and sustainability for powering electronics.

For monitoring the quality of water, a commercial water test pen without a battery was used as the sensor for detecting the TDS in water. Fig. 6f shows the photograph of the self-powered water quality
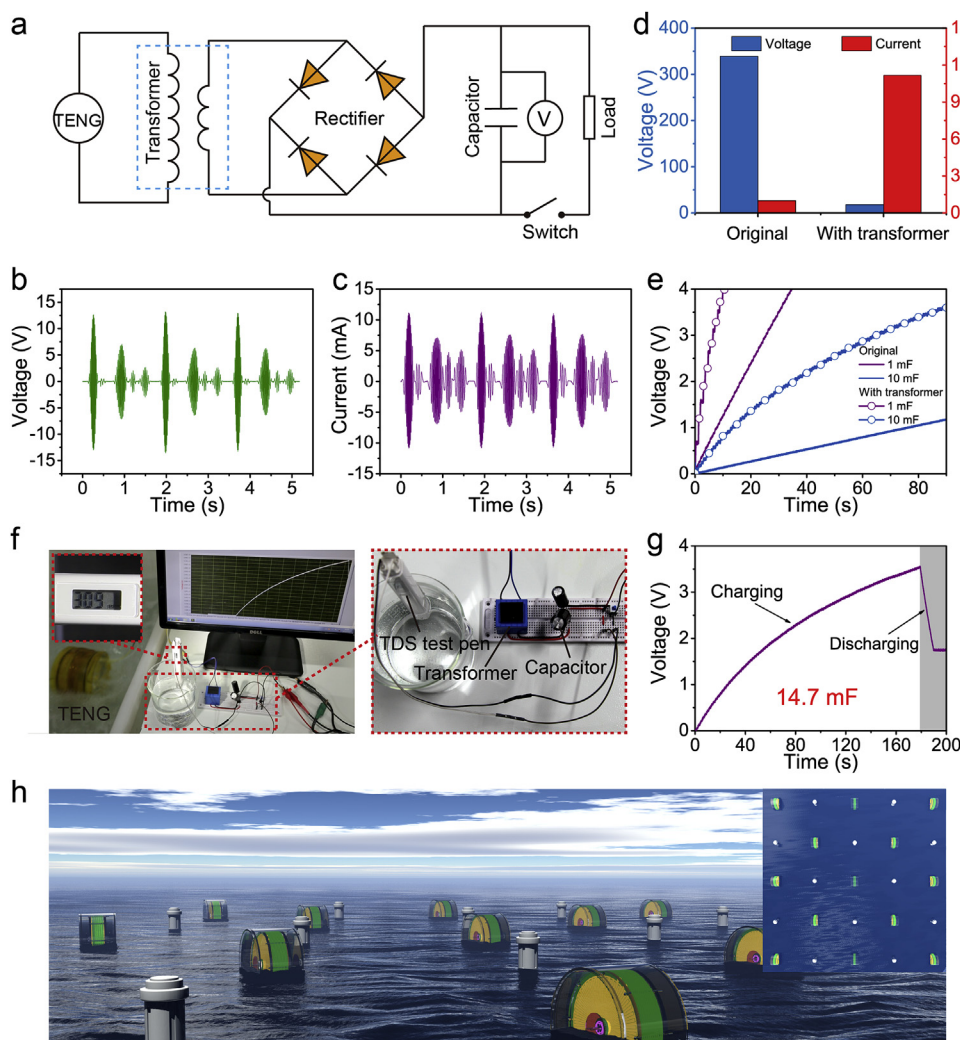


Fig. 6. Power management of the TD-TENG for self-powered TDS test. a) Circuit diagram of the TD-TENG to power electronic devices. b) Open-circuit voltage, and c) short-circuit current of the TD-TENG in water with a transformer connected. d) Comparison of the open-circuit voltage and short-circuit current of the TD-TENG with and without a transformer connected. e) Comparison of the voltage of capacitors charged by the TD-TENG with and without a transformer connected. f) Photograph of the TD-TENG powering a TDS test pen. Inset shows that the TDS test pen displays the right test result. The enlarged photograph shows the power management circuit. g) The charging and discharging profile of the TDS test pen powered by the TD-TENG. h) Schematic of the self-powered, in-situ water quality mapping. Inset shows the vertical view of the array of TD-TENGs and water quality sensors. The wave frequency is 0.58 Hz.

monitoring system. The TDS test pen was connected to the TD-TENG through the power management circuit. In this system, two capacitors were parallel connected, and the total capacitance is 14.7 mF. The charging curve of the capacitors as the system operates is shown in Fig. 6g. Firstly, the capacitor was charged to 3.5 V in 180 s, then the test pen was turned on by closing the switch. The stored electrical energy allowed the test pen to function normally and the TDS of the water was measured as 309 ppm. The whole process is also demonstrated in Video S2. Here, the normal operating voltage and current of the TDS test pen are 3 V and 3 mA, which imply much larger energy consumption than the thermo meter or wireless transmission [17,31]. The realization of the self-powered water quality monitoring system indicates that the TD-TENG is capable for the fabrication of more complicated self-powered systems with high power requirements, which can be adopted widely in various water bodies, especially in ocean where water wave energy is abundant.

Supplementary video related to this article can be found at https://doi.org/10.1016/j.nanoen.2019.104117.

When organized in a network, each TD-TENG can harvest water wave energy locally and supply power for a water quality sensor, thus in-situ and real-time mapping of the water quality in a vast area of water can be achieved, as schematically illustrated in Fig. 6h. The system can provide comprehensive water quality information of the water, not only in temporal but also in spatial dimensions, thus the source and diffusion direction of pollution can be well monitored and analyzed by such self-powered water quality mapping system. It can be further extended to applications in smart ocean with more types of sensors integrated. Considering the low cost in fabrication and maintenance, the TD-TENG should be promising for future ocean research and exploiting, such as wave energy farm and environment protection.

## 3. Conclusions

In summary, a high-power tandem disk triboelectric nanogenerator that can harvest wave energy locally for self-powered water quality monitoring is demonstrated. The device adopts a radial grating disk structure that can convert low-frequency water wave agitations into high-frequency electrical output. A frosted tribo-surface is chosen to solve the challenge of exorbitant friction force that can always prohibit the rotation of such device under slow agitations like water waves, making the rotating grating structure applicable for water wave energy harvesting. With the optimized design, the device exhibits excellent responsivity to low-frequency water waves and boosts the output with a maximum peak power of 45.0 mW and a maximum average power of 7.5 mW in wave tank tests, which are roughly 35 folds and 24 folds of the ball-shell structured device. The average power density reaches 7.3 W m$^{-3}$. The high frequency of the output also facilitates the power management, and the circuit based on a transformer can amplify the output current by about 17 times, which is enough for fast charging large capacitors, reaching the requirements of TDS sensing that has high working current and energy consumption. The self-powered water quality monitoring system is thus successfully fabricated, which can be organized into networks for in-situ, real-time mapping water quality in a large area. The TD-TENG as a high-power water wave energy harvesting device opens up an avenue to solve the bottleneck of power supply for versatile sensing platforms that need to be self-powered and work autonomously in certain water environment, providing a fundamental technology for smart ocean.

## 4. Experimental Section

### 4.1. Fabrication of the TENG

For the stator, the substrate (1 mm in thickness) with two copper layers (35 μm in thickness) on the two sides was fabricated by PCB technics, then PTFE films with a thickness of 80 μm were adhered on

both sides. For the rotator, the frosted acrylic sheet was shaped by a laser cutter (PLS6.75, Universal Laser Systems, USA), and a layer of copper (100 nm in thickness) was deposited on both sides through magnetron sputtering (PVD75 Pro-line, Kurt J. Lesker company, USA). The stators were connected by screws on the edge, and the rotators were connected coaxially by the two shafts in the center with two hanging mass blocks. A pair of bearings were used to mount the shafts. All TENG units and the mass block were sealed in the acrylic chamber.

### 4.2. Characterization

The relative angular displacement was measured by an angular sensor (GT-A-A-2236, WXXY Millay, China). The open-circuit voltage, transferred charges and the current were measured by an electrometer (Keithley 6514, Tektronix Company, USA). The transformer (PE-2818) was purchased from YHDC Electronics. The TDS test pen was purchased from XIAOMI Corporation, China.

## Appendix A. Supplementary data

Supplementary data to this article can be found online at https://doi.org/10.1016/j.nanoen.2019.104117.

## References

[1] R.P. Schwarzenbach, T. Egli, T.B. Hofstetter, U. von Gunten, B. Wehrli, Annu. Rev. Environ. Resour. 35 (2010) 109–136.
[2] M. Shahidul Islam, M. Tanaka, Mar. Pollut. Bull. 48 (2004) 624–649.
[3] V. Cheevaporn, P. Menasveta, Mar. Pollut. Bull. 47 (2003) 43–51.
[4] Z. Wu, J. Liu, J. Yu, H. Fang, IEEE ASME Trans. Mechatron. 22 (2017) 2130–2140.
[5] Y. Qin, A.U. Alam, S. Pan, M.M.R. Howlader, R. Ghosh, N.-X. Hu, H. Jin, S. Dong, C.-H. Chen, M.J. Deen, Sens. Actuators, B 255 (2018) 781–790.
[6] Z. Xu, W. Zhou, Q. Dong, Y. Li, D. Cai, Y. Lei, A. Bagtzoglou, B. Li, Environ. Sci.: Water Res. Technol. 3 (2017) 865–874.
[7] A. Maity, X. Sui, C.R. Tarman, H. Pu, J. Chang, G. Zhou, R. Ren, S. Mao, J. Chen, ACS Sens. 2 (2017) 1653–1661.
[8] F. Adamo, F. Attivissimo, C.G.C. Carducci, A.M.L. Lanzolla, IEEE Sens. J. 15 (2015) 2514–2522.
[9] Z.L. Wang, T. Jiang, L. Xu, Nano Energy 39 (2017) 9–23.
[10] J. Tollefson, Nature 508 (2014) 302–304.
[11] E. Callaway, Nature 450 (2007) 156–159.
[12] F. Fan, Z. Tian, Z.L. Wang, Nano Energy 1 (2012) 328–334.
[13] J. Wang, S. Li, F. Yi, Y. Zi, J. Lin, X. Wang, Y. Xu, Z.L. Wang, Nat. Commun. 7 (2016) 12744.
[14] Z.L. Wang, J. Chen, L. Lin, Energy Environ. Sci. 8 (2015) 2250–2282.
[15] Y. Yang, H. Zhang, J. Chen, S. Lee, T.-C. Hou, Z.L. Wang, Energy Environ. Sci. 6 (2013) 1744–1749.
[16] B. Chen, Y. Yang, Z.L. Wang, Adv. Energy Mater. 8 (2018) 1702649.
[17] L. Xu, T. Bu, X. Yang, C. Zhang, Z.L. Wang, Nano Energy 49 (2018) 625–633.
[18] Y. Bai, C.B. Han, C. He, G.Q. Gu, J.H. Nie, J.J. Shao, T.X. Xiao, C.R. Deng, Z.L. Wang, Adv. Funct. Mater. 28 (2018) 1706680.
[19] J. Nie, Z. Wang, Z. Ren, S. Li, X. Chen, Z. Lin Wang, Nat. Commun. 10 (2019) 2264.
[20] Y. Jie, Q. Jiang, Y. Zhang, N. Wang, X. Cao, Nano Energy 27 (2016) 554–560.
[21] X. Cao, Y. Jie, N. Wang, Z.L. Wang, Adv. Energy Mater. 6 (2016) 1600665.
[22] W. Tang, Y. Han, C.B. Han, C.Z. Gao, X. Cao, Z.L. Wang, Adv. Mater. 27 (2015) 272–276.
[23] S. Niu, Z.L. Wang, Nano Energy 14 (2015) 161–192.
[24] Z.L. Wang, Mater. Today 20 (2017) 74–82.
[25] Q. Zhong, J. Zhong, B. Hu, Q. Hu, J. Zhou, Z.L. Wang, Energy Environ. Sci. 6 (2013) 1779–1784.
[26] L. Xu, H. Wu, G. Yao, L. Chen, X. Yang, B. Chen, X. Huang, W. Zhong, X. Chen, Z. Yin, Z.L. Wang, ACS Nano 12 (2018) 10262–10271.
[27] Z.L. Wang, Faraday Discuss 176 (2014) 447–458.
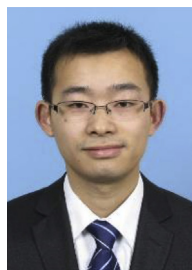[28] Z.L. Wang, Nature 542 (2017) 159–160.

[29] X. Wang, S. Niu, Y. Yin, F. Yi, Z. You, Z.L. Wang, Adv. Energy Mater. 5 (2015) 1501467.
[30] L. Xu, Y. Pang, C. Zhang, T. Jiang, X. Chen, J.J. Luo, W. Tang, X. Cao, Z.L. Wang, Nano Energy 31 (2017) 351–358.
[31] L. Xu, T. Jiang, P. Lin, J.J. Shao, C. He, W. Zhong, X.Y. Chen, Z.L. Wang, ACS Nano 12 (2018) 1849–1858.
[32] X. Zhao, S. Kuang, Z.L. Wang, G. Zhu, ACS Nano 12 (2018) 4280–4285.
[33] G. Zhu, J. Chen, T. Zhang, Q. Jing, Z.L. Wang, Nat. Commun. 5 (2014) 3426.
[34] C. Han, C. Zhang, W. Tang, X. Li, Z.L. Wang, Nano Res. 8 (2014) 722–730.
[35] S.L. Zhang, M. Xu, C. Zhang, Y.-C. Wang, H. Zou, X. He, Z. Wang, Z.L. Wang, Nano Energy 48 (2018) 421–429.
[36] S. Niu, X. Wang, F. Yi, Y.S. Zhou, Z.L. Wang, Nat. Commun. 6 (2015) 8975.
[37] F. Xi, Y. Pang, W. Li, T. Jiang, L. Zhang, T. Guo, G. Liu, C. Zhang, Z.L. Wang, Nano Energy 37 (2017) 168–176.

**Yu Bai** received his undergraduate degree from North China University of Technology in 2015, and his major is Mechanical Engineering. Now he is a Ph.D. candidate in Beijing Institute of Nanoenergy and Nanosystems, Chinese Academy of Sciences. His research interests are focused on air purification, blue energy harvesting, and self-powered systems.

**Dr. Liang Xu** received his Ph.D. degree from Tsinghua University (THU) in 2012, with awards of Excellent Doctoral Dissertation of THU and Excellent Graduate of Beijing. From 2015, he worked as a postdoctoral fellow under the supervision of Prof. Zhong Lin Wang in Beijing Institute of Nanoenergy and Nanosystems (BINN), Chinese Academy of Sciences. He is now an associate professor in BINN. His research interests include triboelectric nanogenerators and self-powered systems, blue energy, fundamental tribological phenomena, scanning probe microscopy and molecular dynamics simulation.

**Dr. Chuan He** is an associate research fellow at School of Materials Science and Engineering, Beijing Institute of Technology. He received his Ph.D. degree in Physics at University of Konstanz in 2015, and did his postdoctoral research under the supervision of Prof. Zhong Lin Wang at Beijing Institute of Nanoenergy and Nanosystems. His current research involves ultrafast dynamics in semiconductor nanostructures, triboelectric nanogenerators, and lithium-ion batteries.

**Laipan Zhu** received his B.S. degree in Physics department from Shandong university in 2010 and his Ph.D. in Institute of Semiconductors, Chinese Academic of Sciences in 2015. Now he is an associate professor in Prof. Zhong Lin Wang's group in Beijing Institute of nanoenergy and nanosystems, Chinese Academic of Sciences. His main research interests have been focused on the field of piezotronics, piezo-phototronics and spintronics.

**Xiaodan Yang** received her Bachelor of Science in Xidian University in 2016. She is currently pursuing a master's degree in Beijing Institute of Nanoenergy and Nanosystems under the supervision of Prof. Zhong Lin Wang. Her research interests include blue energy and self-powered electronics.

**Tao Jiang** received his Ph.D. degree from East China University of Science and Technology in 2014. Now he is an associate researcher in Prof. Zhong Lin Wang's group at Beijing Institute of Nanoenergy and Nanosystems, Chinese Academy of Sciences. His research interests are the theoretical studies of triboelectric nanogenerators, and practical applications in blue energy harvesting and self-powered sensing.

**Jinhui Nie** received his bachelor's degree in Applied Chemistry at Shandong University in 2015. Now he is a Ph.D candidate in Beijing Institute of Nanoenergy and Nanosystem, Chinese Academy of Science. His current research mainly focuses on triboelectric nanogenerators and their applications in energy storage and self-powered micro-fluidic transport system.

**Wei Zhong** received his undergraduate degree in Chemical Engineering and Technology from Jishou University, China in 2015. Now he is a doctoral candidate in Beijing Institute of Nanoenergy and Nanosystems, Chinese Academy of Sciences. His research interests are mainly focused on triboelectric nanogenerators and special materials.

**Prof. Zhong Lin Wang** received his Ph.D. from Arizona State University in physics. He now is the Hightower Chair in Materials Science and Engineering, Regents' Professor, Engineering Distinguished Professor and Director, Center for Nanostructure Characterization, at Georgia Tech. Prof. Wang has made original and innovative contributions to the synthesis, discovery, characterization and understanding of fundamental physical properties of oxide nanobelts and nanowires, as well as applications of nanowires in energy sciences, electronics, optoelectronics and biological science. His discovery and breakthroughs in developing nanogenerators established the principle and technological roadmap for harvesting mechanical energy from the environment and biological systems for powering a personal electronics. His research on self-powered nanosystems has inspired the worldwide effort in academia and industry for studying energy for micro-nano-systems, which is now a distinct disciplinary in energy research and future sensor networks. He coined and pioneered the field of piezotronics and piezophototronics by introducing piezoelectric potential gated charge transport process in fabricating new electronic and optoelectronic devices. Details can be found at: www.nanoscience.gatech.edu.